PROCEEDINGS, 43rd Workshop on Geothermal Reservoir Engineering
Stanford University, Stanford, California, February 12-14, 2018
SGP-TR-213

Geothermal Modeling in Complex Geological Systems with the ComPASS Code

Simon Lopez[1], Roland Masson[2], Feng Xing[1,2], Laurence Beaude[1,2], Nabil Birgle[2], Farid Smai[1], Konstantin Brenner[2], Michel Kern[3], Gabriel Courrioux[1], Severine Caritg[1] and Yannis Labeau[1,4]

1. BRGM, Georesources Division, 3 av. Claude-Guillemin - BP 36009, 45060 Orléans Cedex 02 – France
2. Lab. Jean Alexandre Dieudonné, Université Nice Sophia Antipolis, 06800 Nice Cedex 02 – France
3. INRIA, SERENA, 2 rue Simone Iff, 75589 Paris– France
4. Université des Antilles, Bioshpères, BP 7029, 97275 Schoelcher– France

s.lopez@brgm.fr

Keywords: reservoir modeling, hydrothermal simulations, multiphase flow, unstructured meshes, fracture network

ABSTRACT

Deep geothermal systems often lie in complex geological settings, with multi-scale geological structures that exert a dominant control on convective processes and the transfer of geothermal heat. Methods based on the implicit description of geometrical objects offer an efficient framework to quickly build structural models of such contexts with the occurrence of discontinuities like faults and fractures. Yet, when it comes to discretizing such models the implicit nature of surfaces make volume meshing a non-trivial task and the results are unstructured polyhedral meshes. Over the last few years, much progress has been made towards the consistent and robust discretization of diffusion processes in porous media. These research efforts resulted in several numerical schemes designed with a sound mathematical basis and able to deal with subsurface spatial heterogeneities (permeability variations, anisotropies…) and general polyhedral meshes. We introduce hereafter the ComPASS platform, an open source initiative that aims at building a geothermal simulation platform relying on one such scheme and recent numerical techniques. The current code is able to handle compositional multiphase Darcy flows, relying on a Coats type formulation, coupled to the conductive and convective transfers of energy. Simulations can be run on unstructured meshes including complex networks of fractures with intersecting fractures. Flow inside the fractures is modelled with a so called hybrid-dimensional model, using a 2D model in the fractures that can have variable apertures and permeability and is coupled with 3D transfers in the matrix. The physics is discretized using a fully implicit time integration combined with the Vertex Approximate Gradient (VAG) finite volume scheme. The fully coupled system is assembled and solved in parallel using the PETSc library and can be run on large computing clusters. An efficient preconditioner is implemented to solve the linear systems at each time step and each Newton type iteration of the simulation. A high level interface to describe the simulations is provided by the Python language, whereas the core routine are written in Fortran and C++. This paper reviews the theoretical foundations and presents a few examples of applications along with the current development perspectives.

1. INTRODUCTION

1.1 Towards a better integration of geological and hydrothermal modeling

Deep geothermal energy allows clean, non-intermittent heat and/or power production with very limited environmental impact. It can have a substantial contribution to the decarbonization of our economy (ANCRE, 2015). However, as for all subsurface natural resources, it is faced with the *geological risk*. This makes deep geothermal operations risk to high-risk projects with substantial initial investments related to drilling costs. Even if insurance policies have been set up for long and recently adapted to new targets, an observation of the history of French geothermal development shows that a single exploration failure may deter operators from a region with assumed good potential for several decades.

It has been observed that one of the most efficient way to mitigate this *geological risk* is the collaborative integration of multidisciplinary data and interpretations into a geomodel of the subsurface, or possibly several ones if alternative hypotheses are to be considered (e.g. Calcagno, 2015). Considering that, the main success indicators of a geothermal project are resource temperature and exploitation flowrate, the first goal of such geothermal conceptual models is often the prediction of the spatial distribution of temperature. Yet, as transient convective processes, which are ubiquitous in high temperature magmatic settings, also control the temperature distribution and the *natural state* of sedimentary basins and basement type geothermal plays, the aforementioned conceptual models should be dynamic by nature and integrate the quantitative modeling of subsurface mass and energy transfers.

1.2 Geological static modelling

Various types of multi-scale geological structures exert a dominant control on subsurface convective transfers. Among these, fault zones are ubiquitous in tectonically active areas such as high temperature magmatic settings where they act as corridors with a preferential location of flow, spatial discontinuities and sharp contrasts in petrophysical properties. Their role has also been acknowledged as a major control in the thermal structure of sedimentary basins where they can act as connections between aquifer levels (Magri *et al.*, 2010; Person *et al.*, 2012; Simms and Garven, 2004). Moreover, most of the time, feed zones of geothermal wells are found at the intersection of the well path and fault zones or fractures (Grant and Bixley, 2011). The heterogeneous distribution of aperture and permeability along the fracture surfaces leads an overall reduction of the fracture transmissivity and flow channeling (de Dreuzy *et al.*, 2012), that, in the case of geothermal exploitation, will lead to non-uniform temperature decrease of the reservoir.

Methods based on the *implicit* description of geometrical objects offer an efficient framework to quickly build complex structural models with the occurrence of faults and fractures. Such frameworks are now implemented in commercial off-the-shelf geomodeling software (*e.g.* GeoModeller, Gocad-SKUA, Leapfrog…), yet the modeling of complex fault systems remains a challenging task (Caumon *et al.*, 2015). The approach chosen in the so-called "potential field method" (Calcagno *et al.*, 2008; Lajaunie *et al.*, 1997) is especially intuitive and powerful as fault slip is not prescribed but automatically deduced from available data. Moreover, the facts that they can be entirely parametrized and do not require manual interaction, like so-called explicit methods (Collon and Caumon, 2017), make that implicit modeling methods are particularly well suited for sensitivity studies and the quantitative analysis of uncertainties associated with 3D geological models (de la Varga *et al.*, 2015; Wellmann *et al.*, 2012, 2014).

Yet, when it comes to produce conformable meshes of such complex geological models in order to run dynamic simulations, the implicit nature of surfaces make volume meshing a non-trivial task. Corner-point grids are widely used in the industry but rely on the sampling of the geological models and generate important approximations of the geometries. State of the art meshing algorithms essentially rely on tetrahedral meshes produced with various algorithms. As an example, the Computational Geometry Algorithms Library (CGAL) offers a powerful 3D mesh generation package dedicated to implicit frameworks. Courrioux *et al.* (2012) used these algorithms in the GeoModeller software to produce conformal tetrahedral meshes that exactly match any geological object and its 2D geometrical boundaries (geological interfaces, faults…) or 1D sharp features (surfaces intersection, well paths…).

1.3 Dynamic modelling of hydrothermal flows

The full integration of static and dynamic modeling has long been recognized as an ideal long-term goal and involves a considerable amount of interrelated complex operations. Yet, an unsatisfactory one-way linear workflow is still often observed in day-to-day practice. A practical explanation has long been computational limitations with reservoir engineers forced to develop considerable expertise in workarounds and *tip and tricks* to preserve physical meanings while achieving affordable simulation times. The unfortunate side-effect is often an over-simplification of geological models even though they represent the only modeling level at which the intrinsically complex behavior of the reservoir can be represented.

Indeed, a vast majority of current operational simulations are still performed on cartesian grids. Yet, simulating complex structures is intractable with such grids which do not allow the inclusion of the accurate position of surface discontinuities such as faults or geological interfaces and may lead to so-called *grid orientation effects* (Eymard *et al.*, 2013). Beyond their inherent simplicity, the use of orthogonal grids is linked to the fact that codes have long been using the two points finite volume scheme that shows very interesting numerical properties (Eymard *et al.*, 2014) but require orthogonality constraints. This orthogonality is natural for grids. It is also an intrinsic property of Voronoï tessellations which may be used to perform simulations but need specific adaptations to preserve geological bodies geometries (Freeman *et al.*, 2014).

However, if one wishes to achieve a two-way interaction between static and dynamic models, the geological model must be kept in a consistent and meaningful state so that one can come back to it, modify it and test the effect of its modifications on dynamic processes.

In the following we focus on the description of the ComPASS simulation platform which is currently developed with the goal to be able to efficiently perform flow simulations on large complex domains such as those obtained from the aforementioned discretization of geological models, without simplification of the underlying geological model. Its main specifications are:

- to perform multiphase multicomponent thermal flow simulation on generic 3D unstructured meshes, possibly containing immersed intersecting fractures, without geometric discretization effects such as "grid orientation effects",
- to show good convergence behavior when solving the highly nonlinear physics of multiphase hydrothermal circulations,
- to achieve good scalability properties to take advantage of the multi-core and parallel architectures of current computers and benefit from the ever increasing availability of supercomputers,
- to accurately deal with the abrupt variations of petrophysical properties and distributions generated from geostatistical techniques, including aperture/permeability distributions along fault/fracture surfaces,
- include the possibility to specify a wide range of boundary conditions with complementary conditions with a special focus on the modeling of shallow processes (shallow processes in the vadose zone),
- accurately describe transport phenomena (heat and tracer) in an eulerian framework.

Besides the oil & gas industry standards, there has been several recent initiatives for the development of high temperature geothermal reservoir simulators (Burnell *et al.*, 2015; Cacace and Jacquey, 2017; Driesner *et al.*, 2015) and code comparison studies (White and Phillips, 2015 that focused on E.G.S.). This paper is essentially a summary of recent and ongoing work on the ComPASS platform. It will highlight briefly its main components and characteristics. The reader interested in further details is referred to the bibliography, namely the works by Xing *et al.* (Xing *et al.*, 2017a) for the description of the theoretical and numerical aspects of the modeling of compositional multiphase flows in fractured media, Beaude *et al.* for the integration of complex well architectures (Beaude *et al.*, 2017a) and the specification of complex boundary conditions (Beaude *et al.*, 2017b, 2018). Additional information is also available on http://www.anr-charms.org.

2. THE MODEL AND ITS DISCRETIZATION

2.1 The continuous multiphase multicomponent model

Xing *et al.* (Xing *et al.*, 2017a) detailed the formulation of the compositional model currently implemented in the ComPASS code, which is based on a Coats' type formulation (Coats, 1989) and which extends the work by Eymard *et al.* (2012) to non-isothermal flows. It accounts for an arbitrary nonzero number of components in each phase allowing to model immiscible, partially miscible or fully miscible flows.

$\mathcal{P}$ denotes the set of phases and C denotes the set of components. Each phase $\alpha \in \mathcal{P}$ is described by its non empty subset of components $C^\alpha \subset C$ in the sense that it contains the components $i \in C^\alpha$. It is assumed that, for any component $i \in C$, there is at least one phase that can contain i, *i.e.* the set of phases containing the component i denoted as $\mathcal{P}_i = \{\alpha \in \mathcal{P} | i \in C^\alpha\}$ is non-empty. . The number of phases and number of components are hard-coded for each thermodynamical module along with the previous relations between phases and components which is implemented as the following boolean table:

set of components $C = \{i_1, i_2, i_3, i_4\}$

set of phases $\mathcal{P} = \{\alpha_1, \alpha_2, \alpha_3\}$

	i_1	i_2	i_3	i_4	
α_1	✓		✓	✓	$C^{\alpha_1} = \{i_1, i_3, i_4\}$
α_2		✓		✓	
α_3		✓	✓		
		$\mathcal{P}_{i_2} = \{\alpha_2, \alpha_3\}$			

Table 1: Specification of the relations between phases and components

subcritical pure water

	H_2O
liquid	✓
gas	✓

black-oil model

	water component	*oil component*
water phase	✓	✓
oil phase		✓

Table 2: Example on two simple cases : subcritical pure water (on the left) and so-called black-oil model (on the right)

As the model takes into account phase change reactions which are assumed to be at equilibrium, it results that phases can appear or disappear. The unknown representing the set of present phases is noted $\mathcal{Q} \subset \mathcal{P}$ with $\mathcal{Q} \neq \emptyset$. For a given set of present phases $\mathcal{Q}$, it may occur that a component $i \in C$ does not belong to the subset $\bigcup_{\alpha \in \mathcal{Q}} C^\alpha \subset C$. Hence, we define $\overline{C_\mathcal{Q}}$ the subset of absent components, in the sense that there is no phase in $\mathcal{Q}$ that could contain i (what implies that i can not be present). For example, taking the example of table 1, if $\mathcal{Q} = \{\alpha_2, \alpha_3\}$ we will have $\overline{C_\mathcal{Q}} = \overline{C_{\{\alpha_2, \alpha_3\}}} = \{i_1\}$.

Then, thermodynamical properties of each phase $\alpha \in \mathcal{P}$ depend on the phase pressures P^α, the temperature T, and the phase molar fractions $C^\alpha = \left(C_i^\alpha\right)_{i \in C^\alpha}$. These properties are specified by the user as hard coded functions along with their derivatives.

The formulation relies on the the so-called natural variables and uses the following set of unknowns:

$$X = \left(P^\alpha, T, \left(S^\alpha\right)_{\alpha \in \mathcal{Q}}, \left(C^\alpha\right)_{\alpha \in \mathcal{Q}}, \left(n_i\right)_{i \in \overline{C_\mathcal{Q}}}, \mathcal{Q}\right) \tag{1}$$

where $S = (S^\alpha)_{\alpha \in P}$ is the vector of the phase volume fractions (saturations) and n_i is the number of moles of the component $i \in C$ per unit pore volume. The latest is defined as an independent unknown when $i \in \overline{C_\mathcal{Q}}$ and otherwise given by the formula $n_i(X) = \sum_{\alpha \in \mathcal{Q} \cap \mathcal{P}_i} \varsigma^\alpha \left(P^\alpha, T, C^\alpha\right) S^\alpha C_i^\alpha$ with ς^α being the phase molar density.

Then, one classically writes the molar conservation for each component $i \in C$ and the energy conservation that writes in the form of the following system of P.D.E.:

$$\begin{cases} \phi \partial_t n_i + \nabla \cdot \mathbf{q}_i = 0 \quad i \in C \\ \phi \partial_t E + (1 - \phi) \partial_t E_r + \nabla \cdot \mathbf{q}_e = 0 \end{cases} \tag{2}$$

where t denotes time, ϕ is rock porosity which is assumed to be constant, neglecting mechanical stress, E and E_r are respectively the fluid and rock internal energy per unit rock volume. $\mathbf{q}_i$ denotes the molar flux of component i. It is obtained using a generalized Darcy velocities for each phase $\alpha \in \mathcal{Q} \cap \mathcal{P}_i$ that involves the phase relative permeabilities, dynamic viscosities and the rock intrinsic permeability tensor. $\mathbf{q}_e$ is the energy flux obtained as the sum of an advective component related to the enthalpies of the phases advected by the aforementionned phase Darcy velocities and a diffusive component given by the Fourier law and involving the rock bulk thermal conductivity.

The previous system of conservation equations is finally coupled to the following local closure laws:

$$\begin{cases} \sum_{\alpha \in \mathcal{Q}} S^\alpha = 1 \\ \sum_{i \in C^\alpha} C_i^\alpha = 1 \quad \alpha \in \mathcal{Q} \end{cases} \tag{3}$$

and the thermodynamical equilibrium for each component i present in at least two phases among the set of present phases $\mathcal{Q}$. This equilibrium is currently writen:

$$f_i^\alpha(P,T,C^\alpha)C_i^\alpha = f_i^\beta(P,T,C^\beta)C_i^\beta \quad \alpha \neq \beta \,(\alpha,\beta) \in (\mathcal{Q} \cap \mathcal{P}_i)^2 \;\; i \in \mathcal{C} \tag{4}$$

where f_i^α is the fugacity of component i in phase α. The system is finally completed with an additional equation for the discrete unknown $\mathcal{Q}$ which is typically obtained by a flash calculation:

$$\mathcal{Q} = \mathcal{Q}_{flash}(X) \tag{5}$$

or by simpler criteria depending on the specific thermodynamical system.

2.2 Hybrid model including a discrete fracture network

Two classes of models, dual continuum and discrete fracture models, are typically employed and possibly coupled to simulate flow and transport in fractured porous media. Dual continuum models assume that the fracture network is well connected and can be homogeneized as a continuum coupled to the matrix continuum using transfer functions (*e.g.* the MINC approach in TOUGH2 (Pruess, 1992)). On the other hand, discrete fracture models (DFM), represent explicitly the fractures as codimension one surfaces immersed in the surrounding matrix domain.

ComPASS uses the DFM approach with a lower dimension physical model along the fracture which is derived from the equi-dimensional model of the previous paragraph by integration and averaging along the – possibly variable - width of each fracture. The resulting so-called hybrid-dimensional model couples the 3D model in the matrix with a 2D model in the fracture network taking into account the jump of the normal fluxes as well as additional transmission conditions at the matrix fracture interfaces. These transmission conditions depend on the mathematical nature of the equi-dimensional model and on additional physical assumptions depending on the fracture behavior (drain vs. barrier). The interested reader is referred to the paper by Xing *et al.* (Xing *et al.*, 2017a) for further details.

2.3 Spatial and temporal discretizations

Over the last few years, much progress has been made in the consistent and robust discretization of diffusion processes in porous media. These research efforts resulted in several numerical schemes designed with a sound mathematical framework and able to deal with subsurface spatial heterogeneities (permeability variations, anisotropies…) and general polyhedral meshes. ComPASS currently implements the Vertex Approximate Gradient (VAG) finite volume scheme (Eymard *et al.*, 2012) which belongs to a broader family of numerical scheme called Gradient Schemes (Droniou *et al.*, 2016).

The VAG discretization of hybrid-dimensional two-phase Darcy flows was introduced by Brenner *et al.* (2016) and generalized to multiphase multicomponent flow by Xing *et al.* (Xing *et al.*, 2017a). It considers generalised polyhedral meshes of the simulation domain, which are assumed conforming. The cells are star-shapped polyhedrons, and faces are not necessarily planar in the sense that they can be defined as the union of triangles joining the edges of the face to a so-called *face centre*.

The VAG scheme has different degrees of freedom associated with: cell, cell nodes and fracture face (cf. figure 1). It is a control volume scheme in the sense that it results, for each non Dirichlet degree of freedom, in a molar or energy balance equation. The two main ingredients are therefore the conservative fluxes and the control volumes around degrees of freedom. Figure 1 shows one cell K with one fracture face σ in bold. The matrix fluxes (in blue on figure 1) connect the cell K to the degrees of freedom located at the boundary of K: namely the cell nodes (*e.g.* $F_{K,s}$ and $F_{K,s'}$) and the fracture faces if any (*e.g.* $F_{K,\sigma}$). The fracture fluxes (in red on figure 1) connect each fracture face σ to its nodes (*e.g.* $F_{\sigma,s}$). The expression of the matrix fluxes is linear and local to each cell as the expression of

fracture fluxes is linear and local to each fracture face. Fluxes ensure the cell-cell, cell-fracture face and fracture face-fracture face connections.

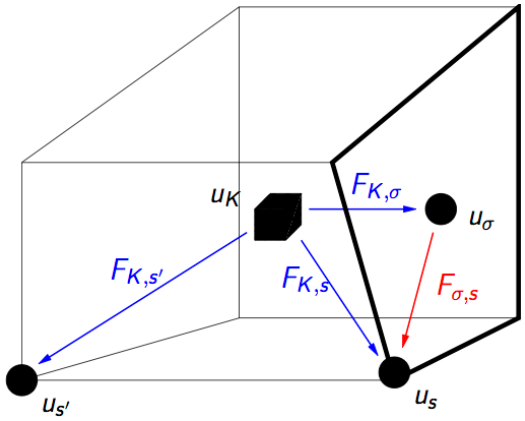

Figure 1: Degrees of freedom and fluxes of the VAG discretization of the hybrid model (cf. text for explanation).

Then, the construction of the control volumes at each degree of freedom is based on partitions of the cells and of the fracture faces: cell (resp. fracture face) volumes are splitted between the cell (resp. fracture face) center and its boundary nodes. In the usual case of cellwise constant rocktypes in the matrix and facewise constant rocktypes in the fracture network, the implementation of the scheme does not require to build explicitly the geometry of these partitions and it is sufficient to define the volume fractions.

As shown in Brenner et al. (2015), the flexibility in the choice of the control volumes is a crucial asset, compared with usual Control Volume Finite Element Methods (CVFE) approaches and allows to significantly improve the accuracy of the scheme when the permeability field is highly heterogeneous. Figure 2, also shows that, as opposed to usual CVFE approaches, this flexibility allows to define the control volumes in the fractures with no contribution from the matrix in order to avoid the artificial enlargement of the flow path in the fractures thus limiting numerical diffusion.

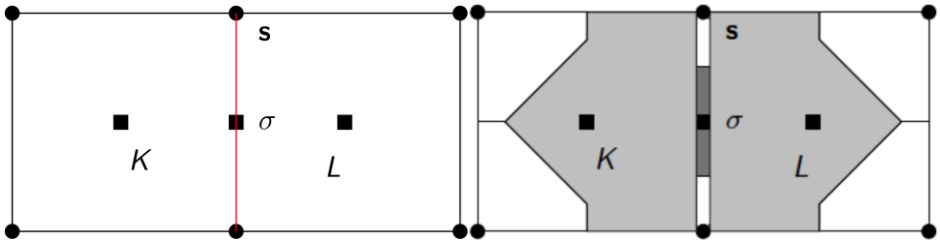

Figure 2: On the left: two cells (K and L) splitted by one fracture face (in red). On the right: example of control volumes associated with the two cells centers (light grey) and with the fracture face center (dark grey) and with (matrix and fracture) nodes (in white). The width of the fracture is enlarged.

To avoid too small control volumes at the nodes located at the fracture intersection, all the fracture faces containing such a node share their volume with it. It results that the control volumes at the fracture intersection nodes are not smaller than at any other fracture degrees of freedom.

The time discretization is based on a fully implicit Euler scheme to avoid severe restrictions on the time steps due to the small volumes and high velocities in the fractures. A phase based upwind scheme is used for the approximation of the mobilities in the Darcy fluxes.

2.4 Non-linear solver

Spatial and temporal discretization of the system of conservation equations (2), including boundary conditions, results in a discrete non linear system $R_\nu(\mathbf{X})=0$ for each degree of freedom with $\mathbf{X}=(X_\nu)_{\nu\in\mathcal{D}}$ denoting the set of all unknowns (1) for all degrees of freedom $\mathcal{D}$ (cells, cell nodes and fracture faces). The problem is closed by adjoining a discrete non linear version $L_\nu(X_\nu)=0$ of the closure laws (3) and thermodynamic equilibrium (4).

Then the non-linear system to be solved at each time step writes in vector form $\mathcal{R}(\mathbf{X})=0$ with:

$$\mathcal{R}(\mathbf{X}) = \begin{cases} R_s(\mathbf{X}) \\ L_s(X_s) \end{cases} \text{for each node } s \quad \begin{cases} R_\sigma(\mathbf{X}) \\ L_\sigma(X_\sigma) \end{cases} \text{for each fracture face center } \sigma \quad \begin{cases} R_K(\mathbf{X}) \\ L_K(X_K) \end{cases} \text{for each cell center } K \tag{6}$$

The non-linear system $\mathcal{R}(\mathbf{X}) = 0$ coupled to the flash fixed point equations (5) expressed locally at each degree of freedom $\mathcal{Q}_\nu = Q_{flash}(X_\nu)$ is solved by an active set Newton-Raphson algorithm (e.g. Coats, 1989) which is detailed by Xing *et al.* (Xing *et al.*, 2017a). For each Newton-Raphson iteration the jacobian matrix is computed:

$$J(\mathbf{X}) = \left.\frac{\partial \mathcal{R}}{\partial \mathbf{X}}\right|_{\mathcal{Q}=Q_{flash}(\mathbf{X})} \tag{7}$$

to solve a linear system of the form:

$$J(\mathbf{X})\Delta_{\mathbf{X}} = -\mathcal{R}(\mathbf{X}) \tag{8}$$

An important point is that the part of the jacobian $J(\mathbf{X})$ of the full system (6) corresponding to the sub-systems $L_\nu(X_\nu) = 0$ appearing in each Newton-Raphson iteration are local to each degree of freedom. Consequently, they can be eliminated straightforwardly by splitting the unknowns between primary and secondary unknowns. Additionally, an interesting property of the VAG scheme is that the part of the jacobian $J(\mathbf{X})$ corresponding to the sub-sybstems $R_K(\mathbf{X}) = 0$ are local to each cell and only involves degrees of freedom located on the cells (cell nodes, cell center and possibly fracture face center). It results that, for each Newton-Raphson iteration, the cell unkwnows can be eliminated too and expressed as linear combinations of the nodes and fracture face unknowns through a Schur complement system. These two successive elimination steps considerably reduce the size of the linear system to be solved for each Newton-Raphson iteration. It makes that the ComPASS implementation of the VAG scheme is particularly efficient on meshes composed mainly of tetrahedrons.

Then, the resulting ill conditioned linear system is solved using an iterative solver (typically GMRES) combined with a preconditioner adapted to the elliptic or parabolic nature of the pressure unknown and to the coupling with the remaining hyperbolic or parabolic unknowns. One of the most efficient preconditioners for such systems is the so-called CPR-AMG preconditioner introduced by Lacroix *et al.* (2001) and Scheichl *et al.* (2003). It combines multiplicatively an algebraic multigrid preconditioner (AMG) for a *pressure block* of the linear system with a more local preconditioner for the full system. Currently, the *pressure equations* defining the *pressure block* are obtained as the sum of the molar conservation equations in each control volume. Then an Incomplete LU factorization of order 0 is used for the full system.

2.5 Wells integration

A first version of reservoir well interaction has been implemented into the ComPASS platform and validated for monophasic cases (Beaude *et al.*, 2017a). Even at a few kilometers scale – typical reservoir scale, the mesh can hardly resolve the well boundary with a radius of the order of 10 cm. Then, the well is modeled as a Dirac source term along the well trajectory. Most well models in reservoir simulations are defined by a set of connected perforations, each perforation belonging to a cell of the mesh (e.g. source block in TOUGH2). In order to take advantage of unstructured meshes and of the nodal feature of the VAG scheme, it is more convenient in our case to discretize each well as a subset of edges of the mesh. This alternative approach provides an efficient way to represent slanted and multi-branch wells. Consequently, wells can easily be taken into account into the mesh generation step by integrating the well paths as additional mesh constraints (e.g. via the *sharp edge features* in the CGAL 3D Mesh Generation Package).

The fluxes connecting the well with the 3D matrix and the 2D fracture network at each node of the well are computed using Peaceman's approach (Chen and Zhang, 2009; Peaceman, 1978, 1983). It is based on a Two Point Flux Approximation (TPFA) with a transmissibility taking into account the unresolved singularity of the pressure (or temperature) solution in the neighborhood of the well. The non-isothermal flow model inside the well is defined using a single implicit unknown for each well corresponding to a reference pressure often coined as the *bottom hole pressure*. The pressures along the well are then deduced from this bottom hole pressure with the crude assumption that the pressure is hydrostatic inside the well. The temperatures along the well are computed assuming thermal equilibrium and a stationary flow inside the well.

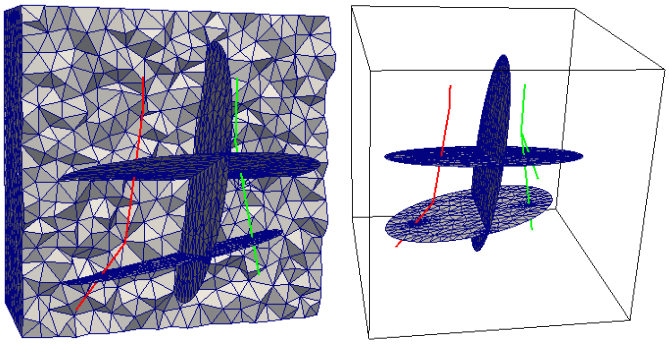

Figure 3: Discretizations of multi-branch (green well) or deviated wells (green and red wells). Each well is discretized as a subset of the edges of the mesh. The tetrahedral mesh is conforming both to 2D elements (fractures – here disks) and 1D elements (domain edges and well paths). Left figure shows both the matrix mesh and the fracture mesh (which are discretized by triangles faces of the matrix tetrahedra). Right figure shows only the fracture triangle mesh and refinement around fracture well intersections.

Then, each new well taken into account is associated with a new unknown and a non linear *well equation*, obtained by the complementary conditions between a specified well mass flow rate (resp. specified exploitation bottom hole pressure) and a specified limit bottom hole pressure (resp. limit well mass flow rate). These new equations are added to the non linear system (6) which is still solved in a fully coupled way, each well equation adding a new line in the linear systems (8).

By connecting all the nodes along the well trajectory to the well reference pressure unknown, the well equation introduces additional connectivity in the system to be solved. This difficulty is to be accounted for in the parallel algorithm that is used to solve it.

2.6 Parallel implementation

The set of cells $\mathcal{M}$ of the mesh is first partitioned into subsets $\mathcal{M}^p$, with p the process rank, using the METIS library (Karypis and Kumar, 1998). In the current implementation, this partitioning is only based on the cell connectivity graph and does not take into account the fracture faces. One layer of ghost cells is added to allow for the synchronization of unknowns between adjacent elements. Nodes and fracture degrees of freedom are then distributed (cf. detail in Xing *et al.*, 2017a), along with well unknowns (details of the distribution are given by Beaude *et al.*, 2017a). The long and short of it is that when wells are present, the degree of freedom corresponding to the well reference pressure is owned by a single process and ghost versions (if not own) of all the well nodes and the well reference pressure are created on any process that has a node in the well path. By doing so, well state can be recomputed locally on any subdomain intersected by the well without communication between processes.

Both the assembly and resolution of linear systems involved in solving the fully coupled non linear system (6) – with additionnal well equations if any - is done in parallel using the Single Program Multiple Data (SPMD). At each Newton-Raphson iteration, a linear system that correspond to rows of the system (8) is built locally on each process p using both own and ghost unknowns and is transfered to the parallel linear solver library PETSc (Balay *et al.*, 2014). The parallel matrix and the parallel vector in PETSc are stored in a distributed manner, i.e. each process stores its own rows. The global linear system is then solved using the GMRES algorithm preconditioned by a CPR-AMG preconditioner as outlined previously. After resolution, the ghost unknowns are recovered by a synchronization step with MPI communications which is efficiently implemented using a PETSc matrix vector product.

3. TEST CASES

The current code repository, versioned with the git software, contain several simple examples and is planned to contain more complex examples that can be found in the bibliography (Beaude *et al.*, 2017a; Xing *et al.*, 2017a, 2017b). We present here the results obtained with a monophasic doublet exploitation of a fractured domain and a diphasic test-case corresponding to the natural state of a synthetic geothermal system as well as preliminary results from a regional scale study. In both test cases the thermodynamic properties of water (liquid and steam) are adapted from the book by Schmidt (1969) but could readily be replaced by any other functions provided that all derivatives are also given by the user.

3.1 Monophasic doublet with fractures

This test case is detailed by Beaude *et al.* (2017a). The simulation domain is defined as a cube with 2 km edges and 3 disk shaped fracture zones. The mesh is a 3D tetrahedral mesh conforming to the fracture network and to the wells (cf. figure 3). It was generated using the implicit framework from the 3D mesh generation package from the Computational Geometry Algorithms Library (CGAL). There is one injection well (red line in figure 3) and one multi-branch production well (green line in figure 3). This mesh contains a little less than 5.10^6 cells, 3.10^4 fracture faces and 8.10^5 nodes. The radius of both wells is set to 10 cm and the fractures are assumed to represent high permeability zones with a constant thickness of 1 m. The permeabilities are isotropic and set to 10^{-14} m^2 in the matrix domain and to 10^{11} m^2 in the fracture network. The porosities are respectively set to 0.1 in the matrix domain and 0.4 in the fractures.

Approximate analytical Peaceman type formulas were used for this test case and were considered to provide a good order of magnitude of the Peaceman indices. The domain is initially set to a uniform temperature of 140°C. At the injection well, a 60°C cold water is injected with a total mass flow rate of 100 t/h and a limit maximum bottom hole pressure of 30 MPa. At the production well, hot water is produced

with the opposite total mass flow rate and a minimum bottom hole pressure of 1 MPa. Figure 4 shows the temperature in the matrix domain and in the fractures after nearly 30 years of continuous exploitation.

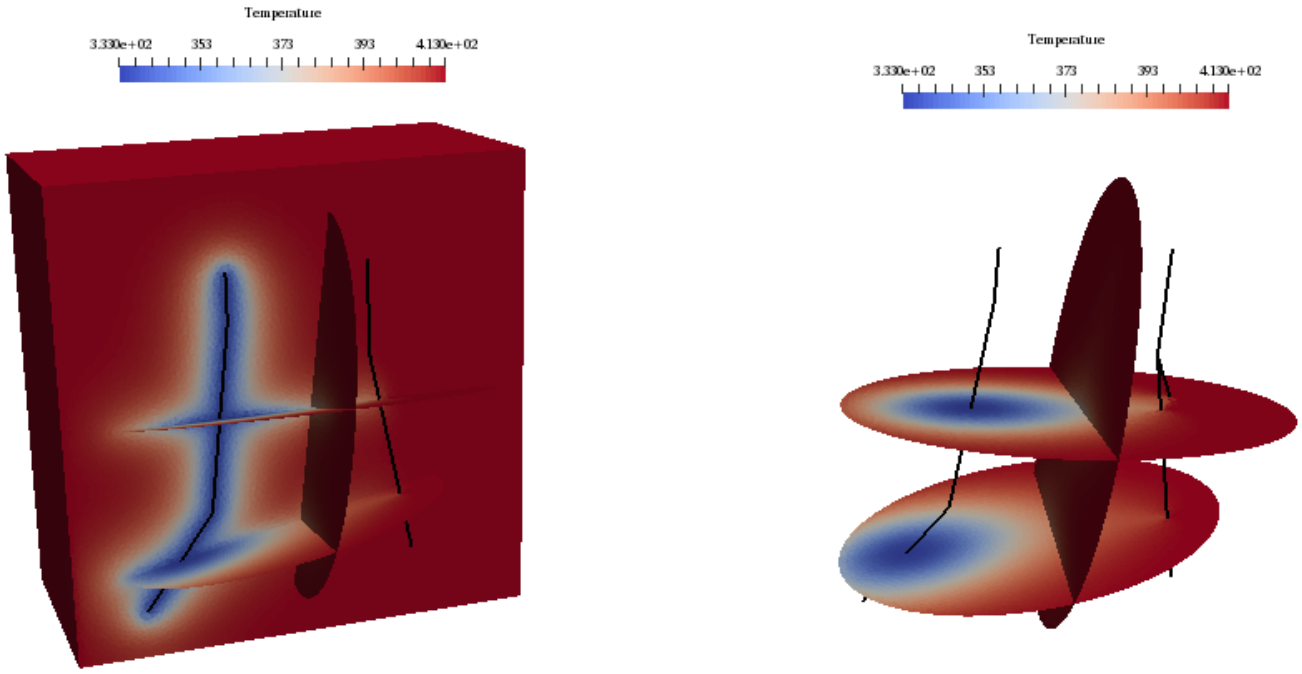

Figure 4: Temperature in K, in the matrix domain (left) and in the fractures (right) after nearly 30 years of continuous exploitation.

3.2 Two-phase subcritical convection

This test case is detailed by Xing *et al.* (Xing *et al.*, 2017a). The simulation domain is a cube with 3 km edges and rectangle shaped fault zones. A conforming tetrahedral mesh was generated with Tetgen (Si, 2015) which is shown in figure 5.

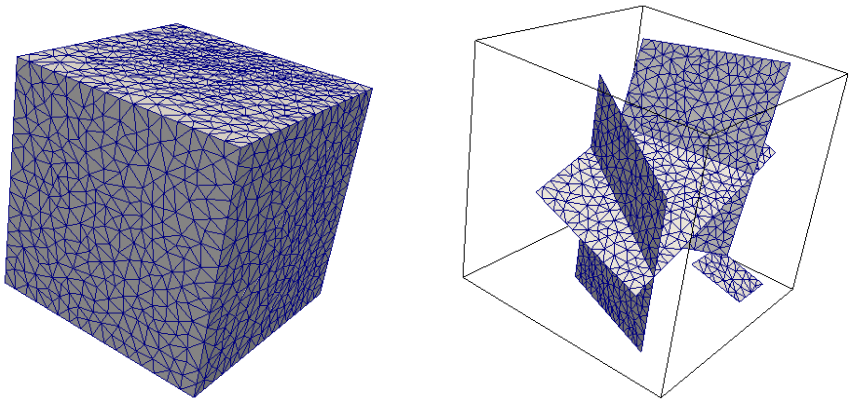

Figure 5: Conforming tetrahedral mesh of the simulation domain (matrix domain on the left, fractures on the right)

The fault zones thicknesses are still fixed to 1 m. Matrix (respectively fracture network) permeability is set to the uniform and isotropic value of 10^{-14} m^2 (respectively 10^{-12} m^2). Matrix (respectively fracture network) porosity is set to 0.25 (respectively 0.35).

At the intersection of the bottom boundary of the domain with the fault network, the temperature is fixed to 450 C and a total mass flow rate of 100 kg/s is prescribed. The matrix bottom boundary is set to 200°C with no flow conditions. The top boundary, is set to atmospheric conditions (1 bar, 20°C) with Dirichlet type conditions so that the fluid is liquid. A zero flux condition for both mass and temperature is imposed at the lateral boundaries of the domain. The simulation domain is initially in liquid phase with a hydrostatic pressure defined by the pressure boundary condition at the top boundary and a linear decrease of the temperature from matrix bottom conditions to surface conditions. Figure 6 shows the temperature in the faults (left) and the gas saturation in the faults and in the matrix domain (right) after 200 years of simulation.

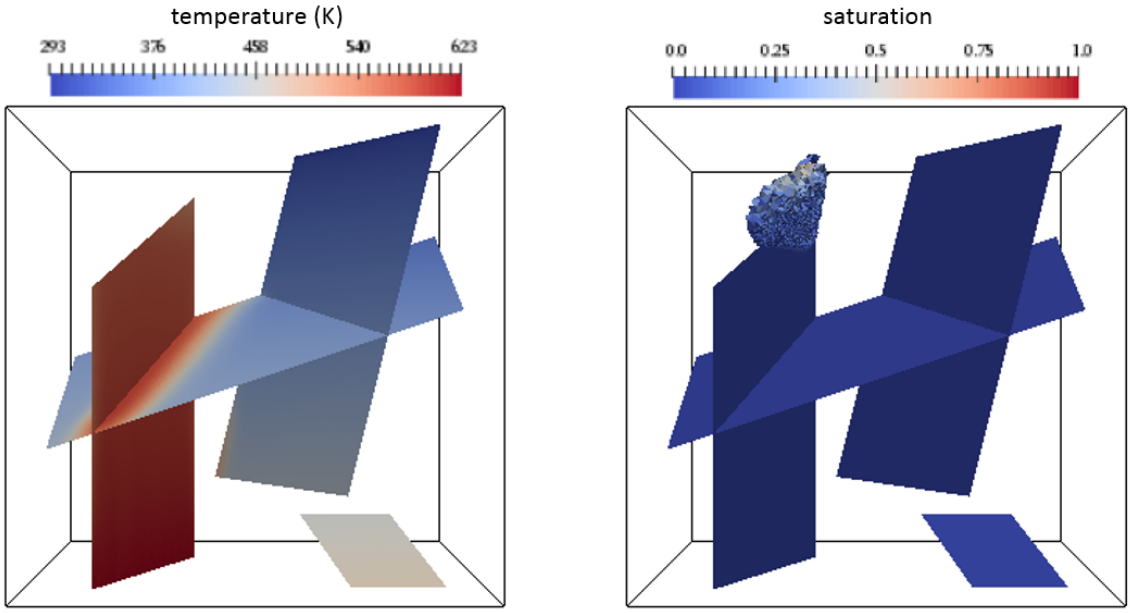

Figure 6: Temperature (K) in the fracture network (left) and steam saturation in both matrix and the fracture (right), after 200 years of simulation. Saturation is clipped to strictly positive values.

3.3 Regional scale simulation

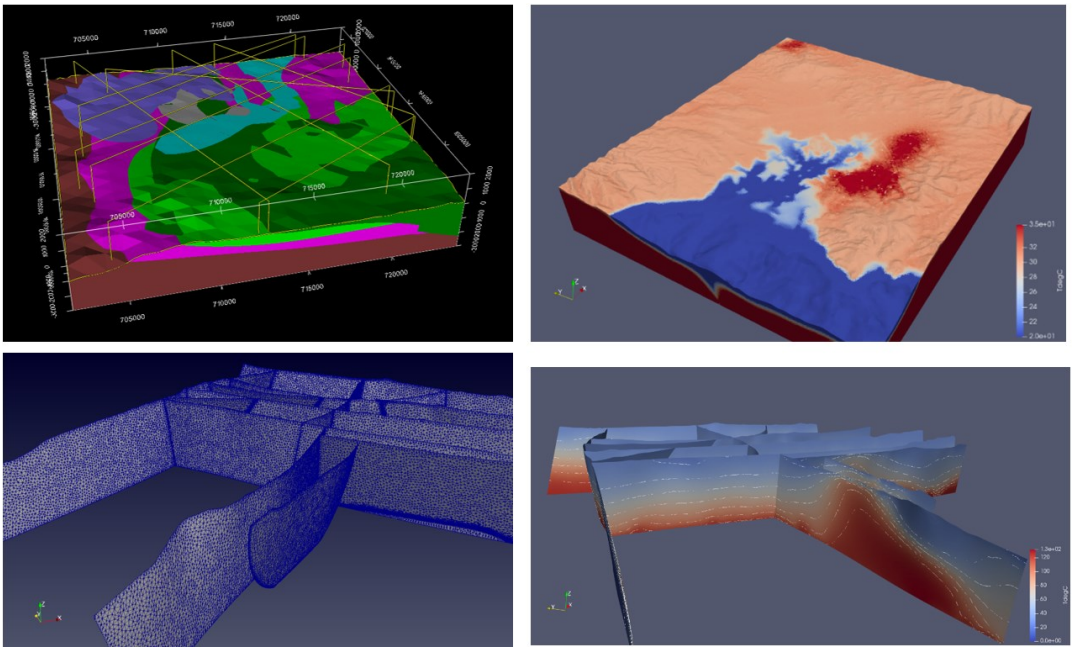

Figure 7: Preliminary results from the modeling of the geothermal potential of the Baie Lamentin area (Martinique). A geological model (upper left) was made then meshed (lower left). Right figures show the yet uncalibrated results of temperature in the matrix (upper right) and the fracture network (lower right).

Figure 7 shows preliminary results from Yannis Labeau Ph.D thesis. A geological model of the Baie Lamentin area (Martinique) that includes several fault zones and volcanic formations was made with the GeoModeller software. A ten million cells conforming mesh was generated using the CGAL libraries (Courrioux *et al.*, 2012). Classical geothermal area conditions were applied with a deep heat source simulated as a temperature Dirichlet conditions and a fracture network which is 3 orders of magnitude more permeable than the surrounding matrix formations. The dynamic model is currently being calibrated to observation data. Each run takes approximately 2 hours on 120 processors on the BRGM computing cluster (5 computing nodes with two AMD Abu Dhabi à 2.6 GHz, 12 cores each and 64 Gb of memory).

4. PERSPECTIVES

4.1 API choices and code development

On the software level we target a modular evolutionary and open framework with a two levels API for the ComPASS platform. The first level targets operational users that want to perform reservoir simulation whether the other one targets numerical engineer and researchers. The version 3 of the ComPASS code was mainly written in Fortran and C++ for the links to the METIS partitioning library and VTK visualization library. Current development version will be released as version 4. It involves a large amount of code refactoring with a shift towards modern C++ and a Python API.

Python is a high level programming language which is widespread amongst the engineering and scientific communities (e.g. Sullivan *et al.*, 2013). It has a lot of efficient libraries designed for scientific work (e.g the NumPy package) and gives the user the ability to write clean, concise and efficient scripts in a natural and understandable way, considerably reducing development cycles. The use of Python does not preclude the use of static form input formats that can directly be managed through the Python interface and data serialization standard/language along with dedicated libraries (e.g. YAML). This option is currently left to the users.

As of today, output of the simulation are performed as compressed binary numpy arrays that can be readily converted to Paraview parallel file formats using provided scripts.

Development is currently performed through INRIA's instance of the Gitlab collaborative platform, under a GPLv3 license. Access to the code can be granted freely upon request at anr-charms@brgm.fr. Several tests are currently defined and gathered for continuous integration.

4.2 Performance and scalability

Version 3 of the ComPASS code benefited from a performance assessment in the context of a joint workshop between the EOCOE and POP centres of excellence for High Performance Computing. The code performed well and potential improvements could be identified.

The current multiphase multicomponent version of the code shows good scalability results (Xing *et al.*, 2017a). However, the scalability of the simulation depends highly on the scalability and the robustness of the preconditioner and linear solver used at each Newton-Raphson iteration. It is well known that AMG type preconditioners require a sufficient number of unknowns per MPI process, say 10,000 as a classical order of magnitude, to achieve a linear strong scaling. For example, on test cases with 2.10^6 unknowns for the pressure block, ComPASS runs show a scalability that is still not far from linear on up to 64 processes and then degrades more rapidly for 128 processes. A detailed instrumentation of the code clearly shows that this degradation is mainly due to the communication overhead. This is consistent with PETSc FAQ accoding to chich "there must be enough work for each process to overweigh the communication time (…) [with] an absolute minimum of about 10,000 unknowns per process, better [being] 20,000 or more."

4.3 Physics

Thermodynamic modules are hard coded in Fortran/C++ so that they can be optimized at compile time. Nevertheless, they can be dynamically loaded at execution, what makes their use quite flexible. We currently implemented in ComPASS, three simple set of thermodynamic properties: subcritical water with relatively simple thermodynamic functions, diphasic module with two components (water and air), and a *black-oil* module (cf. table 2), mainly used for test purposes and benchmarking with oil and gas software. Developments being currently considered are supercritical water/brine (Croucher and O'Sullivan, 2008; Driesner and Heinrich, 2007; Weis *et al.*, 2014) and the inclusion of non condensable gas (Battistelli *et al.*, 2009).

The general multiphase multicomponent framework used in ComPASS makes it relatively straightforward for the user to code new thermodynamic modules provided that he implements the numerical version of the thermodynamic functions he wants to use along with their derivatives. Current improvements of the Python API aim at providing the possibility to explicitly specify equation of states and thermodynamic properties on the Python side to achieve a full configuration of test cases in a high level programing language, without performance loss.

4.5 Boundary conditions

One of the main target of the current developments (cf. also Laurence Beaude et al., 2018) is to overcome several limitations in terms of boundary conditions. Classical choices for boundary conditions are often limited to the following types: fixed value/Dirichlet type for all primary variables or fixed fluxes/Neumann type for all conserved quantities. Mixed-type transient boundary conditions are rarely supported which impedes the convenient modeling of natural processes such as recharge or seepage or water table fluctuations. Workarounds may exist (*e.g.* Hurwitz and Kipp, 2003) but are relatively tedious to implement and are not formulated in a generic way. Transient complex upper or lower boundary conditions could be helpful in taking into account some crucial processes ranging from more realistic heat source modelling to interactions between the vadose zone and fresh water recharge that may hide geothermal resources.

5. CONCLUSIONS

We introduced the open source ComPASS platform which is able to handle compositional multiphase Darcy flows, relying on a Coats type formulation, coupled to the conductive and convective transfers of energy. Simulations can be run on unstructured meshes including complex networks of fractures with intersecting fractures such as those obtained from the discretization of complex geological models. Flow inside the fractures is modelled with a hybrid-dimensional model, using a 2D model in the fractures that can have variable apertures and permeabilities and is coupled with 3D transfers in the matrix. Many of the developments currently performed aim at achieving a

flexible API through a high-level programing language without loss of performances so that geological and dynamic models can be more tightly and easily integrated, leading to both better conceptual models of geothermal systems and operational reservoir models.

ACKNOWLEDGEMENTS

The work of Feng XING who is the main contributor to the version 3 of the ComPASS code was supported by a joint project between INRIA and BRGM Carnot institutes (ANR, INRIA, BRGM). Current developments around the ComPASS code are performed in the framework of the consortium of the CHARMS project between BRGM, Nice Sophia-Antipolis University, Maison de la Simulation, STORENGY and Sorbonne Université (UPMC). The CHARMS project is supported by ANR grant ANR-16-CE06-0009. Laurence BEAUDE's Ph.D grant is jointly supported by BRGM and Région PACA. The Ph.D grant of Yannis Labeau is supported by ADEME Martinique.

REFERENCES

ANCRE (2015). *Decarbonization Wedges*. .

Balay, S. *et al.* (2014). *PETSc User's Manual*. .

Battistelli, A., Carpita, M., Geloni, C. & Marcolini, M. (2009). New TOUGH2 EOS modules for the simulation of geothermal reservoi rs containing saline brines and non - condensable gases. 61032.

Beaude, L., Beltzung, T., Brenner, K., Lopez, S., Masson, R., Smai, F. F., Thebault, J.-F. F. & Xing, F. F. (2017a). Parallel geothermal numerical model with faults and multi-branch wells. *ESAIM: Proceedings and Surveys* **in press**.

Beaude, L., Brenner, K., Lopez, S., Masson, R. & Smai, F. (2017b). Non-isothermal Compositional Two-Phase Darcy Flow: Formulation and Outflow Boundary Condition. *Springer Proceedings in Mathematics and Statistics*. Springer, Cham, 317–325.

Beaude, L., Brenner, K., Lopez, S., Masson, R. & Smai, F. (2018). Numerical Modeling of High Energy Geothermal Systems with Soil Atmosphere Boundary. *43rd Workshop on Geothermal Reservoir Engineering*. Stanford, California, 1–12.

Brenner, K., Groza, M., Guichard, C., Lebeau, G. & Masson, R. (2016). Gradient discretization of hybrid dimensional Darcy flows in fractured porous media. *Numerische Mathematik*. Springer Berlin Heidelberg **134**, 569–609.

Brenner, K., Groza, M., Guichard, C. & Masson, R. (2015). Vertex approximate gradient scheme for hybrid dimensional two-phase Darcy flows in fractured porous media. *ESAIM: Mathematical Modeling and Numerical Analysis* **49**, 303–330.

Burnell, J. *et al.* (2015). Geothermal Supermodels : the Next Generation of Integrated Geophysical , Chemical and Flow Simulation Modelling Tools. *World Geothermal Congress 2015*. Melbourne, Australia, 1–7.

Cacace, M. & Jacquey, A. B. (2017). Flexible parallel implicit modelling of coupled Thermal-Hydraulic-Mechanical processes in fractured rocks. *Solid Earth Discussions* 1–33.

Calcagno, P. (2015). 3D GeoModelling for a Democratic Geothermal Interpretation. *World Geothermal Congres 2015*. Melbourne, Australia, 1–6.

Calcagno, P., Chilès, J.-P., Courrioux, G. & Guillen, A. (2008). Geological modelling from field data and geological knowledge - Part I. *Physics of the Earth and Planetary Interiors* **171**, 147–157.

Caumon, G., Laurent, G., Julio, C., Ford, M. & Godefroy, G. (2015). Fault representations in geomodeling and base formalism. , 102–111.

Chen, Z. & Zhang, Y. (2009). Well flow models for various numerical methods. *International Journal of Numerical Analysis & Modeling* **6**, 375–388.

Coats, K. H. H. (1989). Implicit Compositional Simulation of Single-Porosity and Dual-Porosity Reservoirs. *SPE Symposium on Reservoir Simulation*.

Collon, P. & Caumon, G. (2017). 3D Geomodelling in Structurally Complex Areas - Implicit vs. Explicit representations. *EAGE Conference & Exhibition 2017*, 1–4.

Courrioux, G., Guillen, A. & Bourgine, B. (2012). Tetrahedral meshing of implicit volumes Using CGAL Library. *34th International Geological Congress*.

Croucher, A. E. & O'Sullivan, M. J. (2008). Application of the computer code TOUGH2 to the simulation of supercritical conditions in geothermal systems. *Geothermics* **37**, 622–634.

de Dreuzy, J.-R., Méheust, Y. & Pichot, G. (2012). Influence of fracture scale heterogeneity on the flow properties of three-dimensional discrete fracture networks (DFN). *Journal of Geophysical Research: Solid Earth* **117**, n/a-n/a.

de la Varga, M., Wellmann, F. & Murdie, R. (2015). Adding geological knowledge to improve uncertain geological models: a Bayesian perspective. *Geotectonic Research*. Stuttgart, Germany: Schweizerbart Science Publishers **97**, 18–20.

Driesner, T. & Heinrich, C. A. (2007). The system H2O–NaCl. Part I: Correlation formulae for phase relations in temperature–pressure–composition space from 0 to 1000 °C, 0 to 5000 bar, and 0 to 1 XNaCl. *Geochimica et Cosmochimica Acta,* **71**, 4880–4901.

Driesner, T., Weis, P. & Scott, S. (2015). A New Generation of Numerical Simulation Tools for Studying the Hydrology of Geothermal

Systems to “Supercritical” and Magmatic Conditions. *World Geothermal Congres 2015*. Melbourne, Australia, 1–4.

Droniou, J., Eymard, R. & Herbin, R. (2016). Gradient schemes: Generic tools for the numerical analysis of diffusion equations. *ESAIM: Mathematical Modelling and Numerical Analysis* **50**, 749–781.

Eymard, R., Gallouët, T., Guichard, C., Herbin, R. & Masson, R. (2014). TP or not TP, that is the question. *Computational Geosciences* **18**, 285–296.

Eymard, R., Guichard, C., Herbin, R. & Masson, R. (2012). Vertex-centred discretization of multiphase compositional Darcy flows on general meshes. *Computational Geosciences* **16**, 987–1005.

Eymard, R., Guichard, C. & Masson, R. (2013). Grid Orientation Effect in coupled Finite Volume Schemes. *IMA Journal of Numerical Analysis* **33**, 562–608.

Freeman, C. M., Boyle, K. L., Reagan, M., Johnson, J., Rycroft, C. & Moridis, G. J. (2014). MeshVoro: A three-dimensional Voronoi mesh building tool for the TOUGH family of codes. *Computers & Geosciences*. Elsevier **70**, 26–34.

Grant, M. A. & Bixley, P. F. (2011). *Geothermal Reservoir Engineering (Second Edition)*. Elsevier.

Hurwitz, S. & Kipp, K. L. (2003). Groundwater flow, heat transport, and water table position within volcanic edifices: Implications for volcanic processes in the Cascade Range. *Journal of Geophysical Research* **108**, 1–19.

Karypis, G. & Kumar, V. (1998). A Fast and High Quality Multilevel Scheme for Partitioning Irregular Graphs. *SIAM Journal on Scientific Computing* **20**, 359–392.

Lacroix, S., Vassilevski, Y. V. & Wheeler, M. F. (2001). Decoupling preconditioners in the implicit parallel accurate reservoir simulator (IPARS). *Numerical Linear Algebra with Applications* **8**, 537–549.

Lajaunie, C., Courrioux, G. & Manuel, L. (1997). Foliation Fields and 3D Cartography in Geology : Principles of a Method Based on Potential Interpolation. *Mathematical Geology* **29**, 571–584.

Magri, F., Akar, T., Gemici, U. & Pekdeger, A. (2010). Deep geothermal groundwater flow in the Seferihisar-Balçova area, Turkey: results from transient numerical simulations of coupled fluid flow and heat transport processes. *Geofluids* **10**, 388–405.

Peaceman, D. W. (1978). Interpretation of Well-Block Pressures in Numerical Reservoir Simulation. *Society of Petroleum Engineers Journal*. Society of Petroleum Engineers **18**, 183–194.

Peaceman, D. W. (1983). Interpretation of well-block pressures in numerical reservoir simulation with nonspace grid blocks and anisotropic permeability. *Soc. Pet. Eng.* **23(3)**.

Person, M., Hofstra, A., Sweetkind, D., Stone, W., Cohen, D., Gable, C. W. & Banerjee, A. (2012). Analytical and numerical models of hydrothermal fluid flow at fault intersections. *Geofluids* **12**, 312–326.

Pruess, K. (1992). *Brief Guide to the MINC-Method for Modeling Flow and Transport in Fractured Media.* Lawrence Berkeley Laboratory, University of California.

Scheichl, R., Masson, R. & Wendebourg, J. (2003). Decoupling and Block Preconditioning for Sedimentary Basin Simulations. *Computational Geosciences* **7**, 295–318.

Schmidt, E. (1969). *Properties of water and steam in S.I. units*. Springer-Verlag.

Si, H. (2015). TetGen, a Delaunay-Based Quality Tetrahedral Mesh Generator. *ACM Transactions on Mathematical Software* **41**, 1–36.

Simms, M. A. & Garven, G. (2004). Thermal convection in faulted extensional sedimentary basins: theoretical results from finite-element modeling. *Geofluids* **4**, 109–130.

Sullivan, J. O., Dempsey, D., Croucher, A., Yeh, A. & Sullivan, M. O. (2013). Controlling complex geothermal simulations using PYTOUGH. .

Weis, P., Driesner, T., Coumou, D. & Geiger, S. (2014). Hydrothermal, multi-phase convection of H2O-NaCl fluids from ambient to magmatic temperatures: a new numerical scheme and benchmarks for code comparison. *Geofluids* **14**, 347–371.

Wellmann, J. F., Finsterle, S. & Croucher, A. (2014). Integrating structural geological data into the inverse modelling framework of iTOUGH2. *Computers & Geosciences*. Elsevier **65**, 95–109.

Wellmann, J. F., Finsterle, S., Croucher, A., Engineering, R., Division, E. S., Berkeley, L. & Zealand, N. (2012). Adding Geology To The Equation: Towards Integrating Structural Geological Data Into Inverse Modeling with iTough2. *TOUGH Symposium 2012*, 1–9.

White, M. D. & Phillips, B. R. (2015). Code Comparison Study Fosters Confidence in the Numerical Simulation of Enhanced Geothermal Systems. *Proceedings of 40th Stanford Geothermal Workshop* 1–12.

Xing, F., Masson, R. & Lopez, S. (2017a). Parallel numerical modeling of hybrid-dimensional compositional non-isothermal Darcy flows in fractured porous media. *Journal of Computational Physics* **345**, 637–664.

Xing, F., Masson, R. & Lopez, S. (2017b). Parallel vertex approximate gradient discretization of hybrid dimensional Darcy flow and transport in discrete fracture networks. *Computational Geosciences* **21**, 595–617.